Geometric Brownian information engine: Essentials for the best performance

Rafna Rafeek, Syed Yunus Ali, and Debasish Mondal*
Department of Chemistry and Center for Molecular and Optical Sciences & Technologies, Indian Institute of Technology Tirupati, Yerpedu 517619, Andhra Pradesh, India

(Received 30 March 2022; revised 27 December 2022; accepted 3 April 2023; published 25 April 2023)

We investigate a geometric Brownian information engine (GBIE) in the presence of an error-free feedback controller that transforms the information gathered on the state of Brownian particles entrapped in monolobal geometric confinement into extractable work. Outcomes of the information engine depend on the reference measurement distance x_m, the feedback site x_f, and the transverse force G. We determine the benchmarks for utilizing the available information in an output work and the optimum operating requisites for best achievable work. Transverse bias force (G) tunes the entropic contribution in the effective potential and hence the standard deviation (σ) of the equilibrium marginal probability distribution. We recognize that the amount of extractable work reaches a global maximum when $x_f = 2x_m$ with $x_m \sim 0.6\sigma$, irrespective of the extent of the entropic limitation. Because of the higher loss of information during the relaxation process, the best achievable work of a GBIE is lower in an entropic system. The feedback regulation also bears the unidirectional passage of particles. The average displacement increases with growing entropic control and is maximum when $x_m \sim 0.81\sigma$. Finally, we explore the efficacy of the information engine, a quantity that regulates the efficiency in utilizing the information acquired. With $x_f = 2x_m$, the maximum efficacy reduces with increasing entropic control and shows a crossover from 2 to 11/9. We discover that the condition for the best efficacy depends only on the confinement lengthscale along the feedback direction. The broader marginal probability distribution accredits the increased average displacement in a cycle and the lower efficacy in an entropy-dominated system.

DOI: 10.1103/PhysRevE.107.044122

I. INTRODUCTION

In 1867, Maxwell proposed a hypothetical experiment (Maxwell's demon) that inspects gas molecules in a single heat bath and utilizes the obtained information to extract work, thus apparently violating the second law of thermodynamics [1,2]. Resolution of the paradox unveiled the connection between the thermodynamic entropy and the information gathered from the measurement [3–5]. Szilard's engine, which involves a feedback-controlled measurement process and work that is extracted using the collected information, serves as the foremost benchmark for this apparent paradox [6]. Recently, Sagawa and Ueda provided the quantitative association between entropy and information in the information-fluctuation theorem [7–9], which designates the bound on the work [10] obtained from the available information. These developments spread the notion of information engines, a system that extracts work from a single heat bath using the mutual information earned from the measurement. Execution of a feedback protocol [7–9,11–26], although not limited to Refs. [27–31], is a widely popular mechanism to devise an information engine. Due to their consequences in living systems, several variants of information engines at the mesoscopic level have been studied theoretically, in both classical [12–14] and quantum systems [7,15–17], and validated through experiments [20,22–26]. In many occurrences, a Brownian particle serves as a functional substance [18–23].

Brownian information engines are typically realized by confining particles in monostable or bistable optical traps and implementing an appropriate feedback controller across an operating direction. The upper bound of the achievable work from a Brownian information engine and its optimum functional recipe have been explored recently [21–23]. The capacity of extractable work from such Brownian information engines depends on the strength (frequency) of the confining potential as the latter influences both measurement unpredictability and the relaxation process after the feedback operation. Therefore, the standard deviation of the equilibrium distribution of the particle inside the confining potential plays a central role in determining the best performance prescription. Scrutiny of the total information accumulated through the measurement process and the loss during the relaxation step shows that the Brownian information engine can act as a lossless engine under an error-free estimation [22].

An overwhelming majority of these studies [18–23,32–38] (but not [39]) uses a harmonic or bistable energetic confining potential to set up a Brownian information engine. Therefore, the following questions immediately emerge: (a) Can one actualize a Brownian information engine without external confining potentials? (b) If so, what will be the underlying working principle and performance ability? Recently, we have detailed one of such type, namely a geometrical Brownian information engine [39]. We examined the motion of a free Brownian particle inside a two-dimensional (2D)

*debasish@iittp.ac.in

narrow channel (mesoscopic scale) with varying width across the transport direction. By introducing an appropriate feedback controller, we have determined the upper bound of the extractable work. The particles confined in such geometry with uneven boundaries experience an effective entropic potential along the transport direction. The entropic potential appears as a logarithmic function of the phase-space and is scaled with thermal energy. The equilibrium marginal probability distribution in reduced dimension shapes an inverted parabolic distribution in a purely energy-controlled regime. This affects both the total information gathered during the process and the amount of unavailable information caused by the relaxation process. Consequently, the upper bound of the maximum achievable work from a Brownian information engine in a purely entropy managed condition is less $[(5/3 - 2\ln 2)k_BT]$ [39] than an analogous energetic engine $(k_BT/2)$ [14]. Therefore, it will be interesting to explore the working policy of such a geometric Brownian information engine (GBIE) and its outgrowths in detail, and hence compare the best performance requirements of an entropy-driven information engine with an analogous energetic device. Other than utilizing available information as useful work, the feedback process results in a unidirectional passage of the particle. Thus, analyzing how entropic limitation impacts the average displacement per cycle will also be crucial. The efficacy of an information engine is another factor that warrants attention [9]. The efficacy measures the uses of the information gathered through a measurement and gets influenced by relaxation pathways. The information loss during the relaxation in a GBIE differs from its energetic analog, and it will be exciting to examine how the efficacy develops in increasing entropic control.

In this context, it is noteworthy that the diffusive transport of micro-objects inside a narrow channel has received substantial attention in the recent past [40–60]. Understanding such constrained motion is essential in biological processes such as ions passing through a membrane [61], translocation of polymers through narrow pores [62–64], and chemical reactions in a constrained space [65,66]. Zwanzig derived the theoretical formulation of diffusion inside a restrained channel with irregular boundaries [40]. The diffusion process reduces into a one-dimensional Fick-Jacobs equation in which the effect of varying curvature is considered through an effective entropic potential of the form $k_BT\ln(\Omega(x))$, where $\Omega(x)$ represents the phase-space of the device. Interestingly, a similar type of logarithmic potential appears as a working potential in various biophysical processes, such as optically trapped cold atoms [67–70], DNA unzipping events [71–75], and many others [76–81].

This paper documents the working principles and provisions of the best production of a GBIE. We study a Brownian particle trapped in a two-dimensional monostable spatial confinement and restrained to a constant bias force (G) perpendicular to the longitudinal direction, as shown in Fig. 1 and in the spirit of [39]. The transverse external force G regulates the entropic contribution to the effective potential. We then introduce a feedback controller that consists of three steps: measurement, feedback, and relaxation to complete the cycle, as depicted in Fig. 2. The particle inside the uneven confinement experiences an effective potential

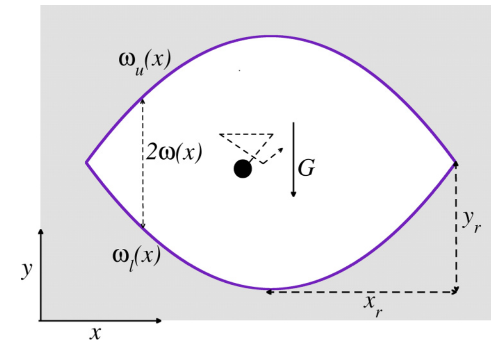

FIG. 1. Schematic illustration of two-dimensional monolobal confinement. $\omega_u(x)$ and $\omega_l(x)$ are the boundary functions of the confinement. x_r and y_r are characteristic length scales that describe the confinement boundary. $\omega(x)$ is the local half-width at x. G denotes the external transverse force acting orthogonal to the feedback direction.

across the feedback direction. Because of the nontrivial interplay between thermal fluctuations, the phase space-dependent effective potential, and the external force (G), the achievements of the information engines would alter significantly for varying measurement distances and feedback locations. We identified the favorable condition in which the device acted as an engine, and we explored the optimum requisites to achieve maximum work. Using the generalized integral-fluctuation relation, we have shown that a GBIE can transform all the available information to output work and, therefore, perform as a lossless information engine. We have also explored the

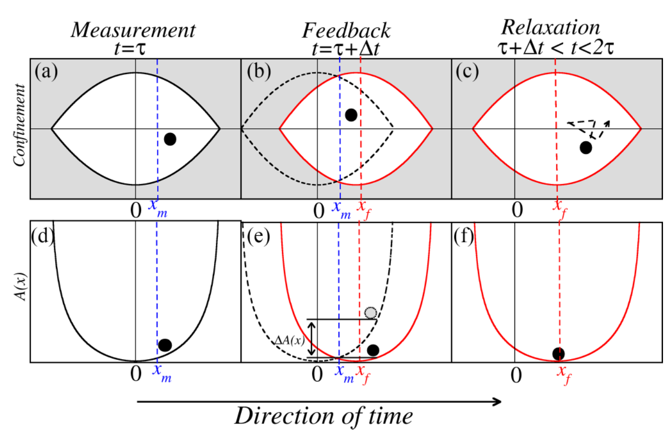

FIG. 2. Schematic representation of a feedback protocol associated with a geometric Brownian information engine (GBIE) during the time interval $\tau \leqslant t \leqslant 2\tau$. The feedback regulator consists of three steps: (a) Measurement: At $t = \tau$, the confinement center is at zero ($\lambda(\tau) = 0$) and we measure the position (x) of the particle. We check whether $x \geqslant x_m$ or not, where x_m is a measurement position (indicated by the vertical blue dashed line). (b) Feedback: If $x \geqslant x_m$, we shift the confinement center instantaneously to the feedback site $\lambda(\tau + \Delta t) = x_f$ (represented by the red solid line). Otherwise, we keep the confinement center unaltered $\lambda(\tau + \Delta t) = 0$. (c) Relaxation: The particle is allowed to relax then with the fixed confinement center at the feedback site (x_f) until the next cycle begins (up to $t = 2\tau$). (d)–(f) Illustration of the feedback regulation in terms of the effective geometric potential.

influence of entropic control on the other important outcomes of the engine, such as the average movement per cycle and the efficacy. We have compared our result with the performance ability of an energetic Brownian information engine and thus gained a thorough understanding of the consequences of the entropic restriction.

II. MODEL AND METHOD

A. Brownian particle in a geometric confinement

We consider a two-dimensional overdamped Brownian particle in a geometric confinement subjected to an external constant force G, acting along the transverse direction (as shown in Fig. 1). Neglecting the inertial force, the dynamics of the particle can be described by the following Langevin equation:

$$\frac{d\vec{r}}{dt} = -G\hat{e}_y + \vec{\zeta}(t), \tag{1}$$

where $\vec{r}$ denotes the position of the particle in two dimensions, $\vec{r} = x\hat{e}_x + y\hat{e}_y$. $\hat{e}_j$ is the unit position vector along the jth direction, and $\vec{\zeta}(t)$ is the Gaussian white noise with the following properties:

$$\begin{aligned} \langle \zeta_j(t)\rangle &= 0 \qquad \text{for } j = x, y,\\ \langle \zeta_i(t)\zeta_j(t')\rangle &= 2D\delta_{ij}\delta(t-t') \quad \text{for } i, j = x, y, \end{aligned} \tag{2}$$

where $D = k_BT$, and $\langle\cdots\rangle$ denotes the averaged realization. We have considered that the frictional coefficient of the particle is unity. The geometric confinement can be generated by imposing noninteractive static boundaries. We describe the upper and lower walls, as depicted in Fig. 1, using the boundary functions $\omega_u(x) = -ax^2 + c$ and $\omega_l(x) = -\omega_u(x)$, respectively, where a and c are constant confinement parameters. Therefore, the lengthscales along the x- and y-directions are x_r $(= \sqrt{c/a})$ and y_r $(= c)$, respectively. The local half-width $\omega(x)$ measures the spatially varying cross-section of the confinement, and they can be written as $\omega(x) = [\omega_u(x) - \omega_l(x)]/2$. The alternative Fokker-Planck description of the process [Eqs. (1) and (2)] can be expressed as [44–46,82–84]

$$\begin{aligned} \frac{\partial}{\partial t}p(x,y,t) &= D\frac{\partial}{\partial x}\left\{e^{\frac{-\psi(x,y)}{D}}\frac{\partial}{\partial x}e^{\frac{\psi(x,y)}{D}}p(x,y,t)\right\}\\ &\quad + D\frac{\partial}{\partial y}\left\{e^{\frac{-\psi(x,y)}{D}}\frac{\partial}{\partial y}e^{\frac{\psi(x,y)}{D}}p(x,y,t)\right\}, \end{aligned} \tag{3}$$

where $\psi(x,y) = Gy$ is a potential function and $p(x,y,t)$ is the probability distribution function of a particle in (x,y) at time t. When the lengthscale along the x-direction (x_r) is much larger than that along the y-direction (y_r), one can assume a fast local equilibrium along the y-direction [40,41]. In this context, we define a position-dependent potential function $A(x)$ as

$$\exp\left(\frac{-A(x)}{D}\right) = \int dy \exp\left(\frac{-\psi(x,y)}{D}\right). \tag{4}$$

If $\rho(y;x)$ is a conditional local equilibrium distribution of y for a given x, and $\rho(y;x)$ is normalized to unity in y, one can write

$$\rho(y;x) = \exp\left(\frac{A(x)}{D}\right)\exp\left(\frac{-\psi(x,y)}{D}\right). \tag{5}$$

The fast-local equilibrium approximation along the transverse direction guides us to [40–44]

$$p(x,y,t) \simeq \rho(y;x)P(x,t), \tag{6}$$

where we express the marginal probability distribution function $P(x,t)$ as

$$P(x,t) = \int_{\omega_l(x)}^{\omega_u(x)} p(x,y,t)dy. \tag{7}$$

Using Eqs. (4)–(7), the two-dimensional Smoluchowski Eq. (3) reduces to a Fick-Jacobs equation in reduced dimension [40–57]:

$$\frac{\partial}{\partial t}P(x,t) = \frac{\partial}{\partial x}\left\{D\frac{\partial}{\partial x}P(x,t) + A'(x)P(x,t)\right\}, \tag{8}$$

where $A(x)$ is the effective potential experienced by the particle in reduced dimension. The effective potential represents the free energy of a particle (at position x) in reduced dimension. $A(x)$ will be of the form

$$A(x) = -D\ln\left[\frac{2D}{G}\sinh\left(\frac{G\omega(x)}{D}\right)\right]. \tag{9}$$

Thus, the effective potential depends on the external transverse force G, the thermal energy D, and the geometry of the confinement in a nontrivial way. In the limit of $G/D \gg 1$, the effective potential reduces to $A(x) = -G\omega(x)$ and is popularly denoted as an energy-dominated situation. In the opposite limit, $G/D \ll 1$, the effective potential becomes independent of G with a logarithmic form, and the potential is purely entropic in nature,

$$\begin{aligned} A(x) &= -G\omega(x) \qquad \text{for } \frac{G}{D} \gg 1,\\ &= -D\ln[2\omega(x)] \quad \text{for } \frac{G}{D} \ll 1. \end{aligned} \tag{10}$$

B. GBIE: Feedback protocol

We construct an information engine consisting of Brownian particles trapped in geometric confinement and subjected to a feedback control as illustrated in Fig. 2. Each cycle consists of three steps: measurement, feedback and relaxation. As there is no real force along the transport direction, the particle does not perform any work of itself. Particles are transported due to changes in the confinement center along the direction of feedback. Therefore, we will use the concept of effective potential $[A(x)]$ to calculate the extractable work equivalence during the feedback protocol. During such feedback, the effective potential experienced by the particle in reduced dimension changes with a change in the confinement center. This present study identifies this net change in effective potential energy as achievable work. Now, as shown in the lower panel of Fig. 2, the particle, confined in a monolobal trap with uneven $\omega(x)$ along x direction, experiences an effective potential $A(x - \lambda(t))$, where the x is the position of the particle, $\lambda(t)$ is the center of the confinement at time t. Initially, we take $\lambda(0) = 0$. Once the thermal equilibrium is reached, i.e., at $t = \tau$, we perform a "measurement" to determine the position of the particle x. We define a reference measurement distance at x_m. If the particle crosses the measurement distance ($x \geqslant x_m$), we shift the confinement center instantaneously to x_f [i.e., $\lambda(\tau + \Delta t) = x_f$ and $\Delta t \to 0$]. In other words, the position of the effective potential center also changes to x_f. Otherwise ($x < x_m$), we leave the confinement center unaltered [i.e., $\lambda(\tau) = 0$]. In this scenario, we do not employ any feedback ($x_f = 0$), and the center of the effective potential remains unchanged. After the feedback, the particle relaxes with fixed $\lambda(\tau)$ until the next feedback. We set the time scale of the feedback protocol τ is much larger than the characteristic relaxation time scale of the system ($\tau \gg \tau_r$). As the shift is instantaneous (error-free) and particles always return to the equilibrium state, the change in the potential energy can fully be converted into work. Therefore, the extractable work $-W(x)$ related to the measurement process can be written as

$$\begin{aligned} -W(x) &= A(x) - A(x - x_f) \quad \text{if } x \geqslant x_m \\ &= 0 \quad\quad\quad\quad\quad\quad\quad\;\; \text{if } x < x_m. \end{aligned} \tag{11}$$

Notably, the effective entropic potential $[A(x)]$ accounts for the free energy associated with the particle in reduced dimension. In thermodynamics, the free-energy change is considered equivalent to extractable work. Therefore, the net change in effective entropic potential on shifting the confinement center is possible extractable work. Here, we note that the total energy change of the particle differs from the change of the effective potential during the change in the confinement center. In an energetic limit ($\frac{G}{D} \gg 1$), the change in total energy and the effective potential on the shifting center coincide with each other. However, in an entropic regime ($\frac{G}{D} \ll 1$), the total energy possessed by the particle is different from the effective potential (calculations not shown here). The process is repeated and the average extractable work is obtained as

$$-\langle W \rangle = -\int_{-x_r}^{x_r} dx\, P_{\text{eq}}(x) W(x), \tag{12}$$

where $x_r = \sqrt{c/a}$ is the confinement length scale along the x-axis and $P_{\text{eq}}(x) = \lim_{t\to\infty} P(x, t)$ is the equilibrium marginal probability distribution. It is worthwhile to mention that $A(x)$ is not a physical potential energy and does not contribute a force field in original 2D Langevin dynamics [Eq. (1)]. However, as mentioned earlier, $A(x)$, experienced by the particle in reduced dimension, changes with a change in the confinement center. During the feedback, we identify this change $A(x)$ as achievable work ($\langle W \rangle$). Later, we will connect this $\langle W \rangle$ to the available or useful information in an error-free feedback environment (which will be discussed later).

Next, we evaluate the net information acquired to examine the upper bound of the extractable work. The term *information* is related to the uncertainty of occurrence or surprisal of a certain event. Information related to an event Y increases as the probability of the same $[P(Y)]$ decreases. When $P(Y)$ tends to unity ($\sim$1), the surprisal of the event is almost zero. On the other hand, if $P(Y)$ is extremely low (close to zero), the surprisal of the event diverges. Therefore one can define the information related to an event Y as $I(Y) = -\ln(P(Y))$. In the present study, we consider an error-free feedback mechanism. In this situation, the net information grossed is equivalent to the Shannon entropy of the particle at initial equilibrium since the Shannon entropy after the measurement is zero. Therefore for an error-free measurement process, the information can be expressed as [9,14,39]

$$\langle I \rangle = -\int_{-x_r}^{x_r} dx\, P_{\text{eq}}(x) \ln[P_{\text{eq}}(x)]. \tag{13}$$

To estimate the unavailable information, we consider the reverse protocol: The particle is initially in equilibrium with the confinement location at $\lambda(t) = x_f$, and we shift the center back to $\lambda(t) = 0$ suddenly irrespective of the position of the particle. For an error-free (almost) measurement, the average unavailable information is [9,14,39]

$$\begin{aligned} \langle I_u \rangle = &-\int_{-x_r}^{x_m} dx\, P_{\text{eq}}(x) \ln[P_{\text{eq}}(x)] \\ &-\int_{x_m}^{x_r} dx\, P_{\text{eq}}(x) \ln[P_{\text{eq}}(x - x_f)]. \end{aligned} \tag{14}$$

The unavailable information ($\langle I_u \rangle$) is an important quantity since it limits the possible extractable work. A higher $\langle I_u \rangle$ lowers the achievable work. We refer the reader to Ref. [14] for further details on total information and the unavailable information related to an event. In the present study, one can calculate both $\langle I \rangle$ and $\langle I_u \rangle$ by estimating the equilibrium marginal probability distribution $[P_{\text{eq}}(x)]$ from the 2D Langevin dynamics [Eq. (1)]. The other physical observable of interest is the efficacy (γ) of the feedback control. The γ measures how efficiently the device utilizes the net acquired information in the feedback protocol. Using the concept of the generalised Jarzynski equality [10,21–23], γ can be written as

$$\gamma = \langle \exp(-\beta W) \rangle = \int_{-x_r}^{x_m} dx\, P_{\text{eq}}(x) + \int_{x_m}^{x_r} dx\, P_{\text{eq}}(x - x_f) \tag{15}$$

for an error-free measurement protocol. Finally, the average step ($\langle \Delta x \rangle$) per feedback cycle can be calculated as

$$\langle \Delta x \rangle = x_f \int_{x_m}^{x_r} dx\, P_{\text{eq}}(x). \tag{16}$$

To proceed further, we discuss the ranges of the measurement (x_m) and feedback positions (x_f). In the present context, the measurement position can be set at any allowed position inside the confinement along the x-direction, $-x_r < x_m < x_r$. Noticeably, the particle can never reach the terminal position $\pm x_r$ precisely. The associated uncertainty and hence the information is undefined for $x_m = \pm x_r$. Thus, to avoid the singularity of the problem, one needs to shift the limit of associated measurement position by $\pm\Delta$ ($\Delta \to 0$), whenever required. We encounter such a singularity problem only in the case of $-\langle W \rangle$ and $\langle I \rangle$ calculated in the entropy-dominated limit ($G/D \ll 1$). In all other scenarios, this singularity problem does not arise. Therefore, we set the extreme points as the concerning limits to make the calculation easier (without any estimation error). Next, we vary the feedback location of the confinement center (x_f) within the range of $0 < x_f < (x_r + x_m)$. In principle, one can choose x_f on the other side of the confinement as well, i.e., $0 > x_f > -(x_r + x_m)$. However, because of the reflection symmetry of the confined structure, the effective potential, and hence the amount of extractable work, is identical for $x_f = \pm x'$. Finally, we assumed that the boundary walls are noninteractive and do not exert any

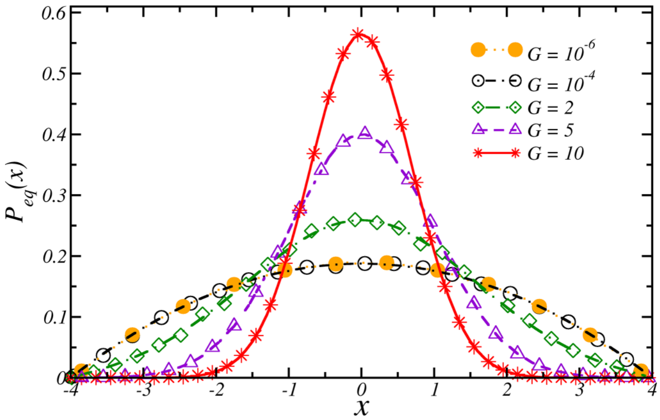

FIG. 3. Variation of equilibrium probability distribution function $P_{\mathrm{eq}}(x)$ with the position x for different values of transverse bias force G. Points are obtained from the numerical simulation study [using Eqs. (1) and (2)] and the lines represent theoretical predictions [using Eq. (17)]. The parameter set chosen is $D = 1$, $a = 0.1$, and $c = 1.6$ for all cases.

force on the particle during a collision. In this regard, we mention that the particle may hit the wall sometime during the feedback protocol (like for $x_f > 2x_m$ and when $x_f > x_m + x_r$). We assume that the "hitting" incidents are weak and cannot change the temperature of the heat reservoir. However, these hitting incidents can only provide a transient effect on the dynamics of the particle and cannot alter $P_{\mathrm{eq}}(x)$. Therefore, such "hitting" events do not affect the estimation of $\langle I\rangle$ or $\langle I_u\rangle$.

C. Numerical simulation details

We understand that the estimation of most of the physical observables under consideration involves the calculation of the equilibrium probability distribution function [$P_{\mathrm{eq}}(x)$]. We solve the Langevin dynamics [Eqs. (1) and (2)] inside the boundary walls using an improved Euler method [85] with a time step ($\Delta t = 10^{-3}$) to find a two-dimensional probability distribution in a long time [$p(x, y, t \to \infty)$]. We consider a reflecting boundary condition near the confinement walls and employ a Box-Muller algorithm to generate the required thermal noise [86]. We obtain $P_{\mathrm{eq}}(x)$ by calculation of the marginal equilibrium distribution function using Eq. (7). For this purpose, we use a spatial grid size of 10^{-1} units. We generate a large number of trajectories ($\sim 10^7$) to obtain a smooth distribution function. To perform numerical integration, we use a trapezoidal rule with a grid size of 10^{-3}, whenever it is required. Unless mentioned otherwise, we set $a = 0.1$, $c = 1.6$, and $D = 1$ throughout the manuscript. Before we proceed, we must mention that one needs to be careful in introducing reflecting boundary conditions for a Brownian particle inside a confined chamber with a hard wall, as addressed in [87]. The time step chosen here is small enough to account for the corrections related to such hard-wall interactions. Also, we consider a low curvature of the boundary wall with centrosymmetric confinement to minimize the numerical error. The agreement between the numerical simulation data of the marginal probability distribution and the same obtained from the Fick-Jacobs approximation, as shown in Fig. 3, validates the choice of the time step.

III. RESULTS AND DISCUSSION

A. Testament to the Fick-Jacobs approximation

The amount of achievable work, the average displacement per cycle, and the efficacy are key physical outcomes of the GBIE. As is evident from the definitions [Eqs. (12)–(16)], we need to assess the equilibrium probability distribution [$P_{\mathrm{eq}}(x)$] of the unshifted confinement [$\lambda(\tau) = 0$] for the theoretical estimation of these observables. One can obtain $P_{\mathrm{eq}}(x)$ by numerically solving the underlying 2D Langevin dynamics [Eqs. (1) and (2)] as mentioned earlier. For an analytical estimation of $P_{\mathrm{eq}}(x)$, we make use of the equilibrium solution of the Smoluchowski equation [Eq. (8)] in reduced dimension, which can be written as [39]

$$P_{\mathrm{eq}}(x) = N \exp\left[\frac{-A(x)}{D}\right], \quad \text{where} \quad N^{-1} = \int_{-x_r}^{x_r} dx\, P_{\mathrm{eq}}(x), \tag{17}$$

where N is the normalization constant. Using Eqs. (10) and (17), one can find the $P_{\mathrm{eq}}(x)$ under a different extent of entropic control:

$$\begin{aligned} P_{\mathrm{eq}}(x) &= \sqrt{\frac{Ga}{\pi D}} \exp\left(-\frac{Ga}{D}x^2\right) \quad \text{for} \quad \frac{G}{D} \gg 1 \\ &= \frac{3}{4}\sqrt{\frac{a}{c^3}}(-ax^2 + c) \quad \text{for} \quad \frac{G}{D} \ll 1. \end{aligned} \tag{18}$$

It must be noted that an assumption of a fast local equilibrium along the transverse direction is necessary for mapping the original two-dimensional Fokker-Planck description [Eq. (3)] into a reduced one-dimensional Smoluchowski equation [Eq. (8)]. Therefore, the applicability of the theoretically obtained $P_{\mathrm{eq}}(x)$ [Eqs. (17) and (18)] is subjected to the validity of the Fick-Jacobs approximation in the considered parameter space. In Fig. 3, we outline the variation of the initial steady-state probability distribution function [$P_{\mathrm{eq}}(x)$] for different transverse force G. Numerical integration of Eqs. (9) and (17) provides the theoretical predictions for an arbitrary value of G. Two limiting conditions in the transverse force, i.e., $G/D \gg 1$ and $G/D \ll 1$, $P_{\mathrm{eq}}(x)$ can be calculated by using Eq. (18). All points in Fig. 3 correspond to Langevin dynamics simulation data. We obtain a good agreement between the theoretical predictions and numerical simulation data. Thus, the Fick-Jacobs approximation is endorsed in reduced dimension.

Figure 3 also depicts that for a high value of external transverse force (here $G = 10$), $P_{\mathrm{eq}}(x)$ is a symmetric Gaussian-like function with $\sigma = \sqrt{D/2Ga}$, where σ is the standard deviation of the probability distribution, and it can be defined as

$$\sigma^2 = \int_{-x_r}^{+x_r} x^2 P_{\mathrm{eq}}(x) dx - \left(\int_{-x_r}^{+x_r} x P_{\mathrm{eq}}(x) dx\right)^2. \tag{19}$$

In the other extreme ($G \to 0$), $P_{\mathrm{eq}}(x)$ spreads out to a symmetric inverse parabolic function and is independent of G. The concerned standard deviation reads $\sigma = \sqrt{c/5a}$.

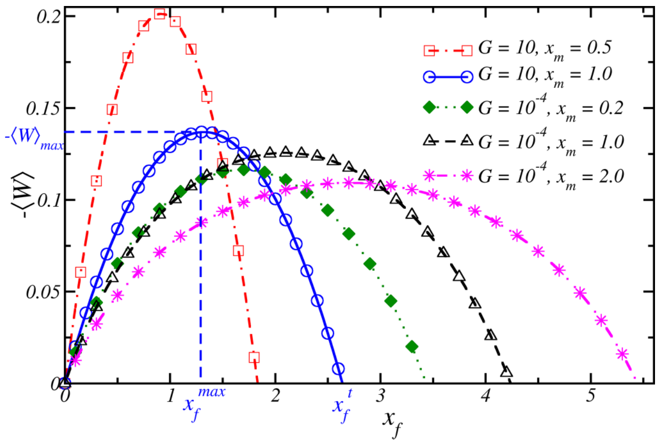

FIG. 4. Variation of average extractable work ($-\langle W\rangle$) during the feedback cycle with the feedback location (x_f) for different values of measurement position (x_m) and different G, following Eqs. (10)–(12) and (17). The parameter set chosen is $D = 1$, $a = 0.1$, and $c = 1.6$ for all cases.

B. Recipe to pull off maximum extractable work ($-\langle W\rangle$)

For a given geometric constraint, the measurement distance x_m and the feedback location x_f designate the feedback protocol and hence the outcomes of the GBIE. Also, the dominance of the transverse bias force (G) governs the supplement due to the entropic restraint. Therefore, we examine the adaptation of the averaged extractable work per cycle, $-\langle W\rangle$, as a function of the feedback location x_f for different measurement distances x_m and G. Using Eqs. (9)–(12) and (17), one can estimate the average extractable work $-\langle W\rangle$ under any irrational geometric restriction. The outcomes are shown in Fig. 4, and the following observations are perceived:

(a) For a given measurement distance x_m and transverse force G, the magnitude of extractable work ($-\langle W\rangle$) shows a turnover with the feedback distance x_f. A maximum extractable work ($-\langle W\rangle_{\max}$) can be achieved for an intermediate feedback location, say $x_f = x_f^{\max}$.

(b) The magnitude of $-\langle W\rangle_{\max}$ changes with x_m nonmonotonically. When all other parameters are kept unchanged, one can realize the highest value of $-\langle W\rangle_{\max}$ for an optimum measurement distance.

(c) One can witness a rise in $-\langle W\rangle_{\max}$ with increasing G. Thus, the maximum extractable work for a given protocol and confinement parameters is higher in the energetic limit than the entropic one.

(d) Finally, the monostable geometric trap can serve as an information engine ($-\langle W\rangle > 0$) only up to a specific value of the feedback position. We observe that the extractable work is not possible beyond $x_f > 2x_f^{\max}$ for any arbitrary system parameter. To apprehend the underlying physics of the observations stated above, we now look into the optimal operating condition on x_m and x_f for maximum extractable work. In the limit of high transverse force ($G/D \gg 1$), one can get the expression of $-\langle W\rangle$ as

$$-\langle W\rangle = \sqrt{\frac{GaD}{\pi}}x_f \exp\left(-\frac{Ga}{D}x_m^2\right) - \frac{Ga}{2}x_f^2 \mathrm{erfc}\left(\sqrt{\frac{Ga}{D}}x_m\right), \tag{20}$$

where $\mathrm{erfc}(z) = 1 - \mathrm{erf}(z)$ is the complementary error function, and $\mathrm{erf}(z) = 2\pi^{-1/2}\int_0^z e^{-y^2}dy$. The solution of $\partial\langle W\rangle/\partial x_f = 0$ with unaltered measurement position x_m yields

$$x_f^{\max} = \sqrt{\frac{D}{Ga\pi}}\frac{\exp\left(-\frac{Ga}{D}x_m^2\right)}{\mathrm{erfc}\left(\sqrt{\frac{Ga}{D}}x_m\right)}, \tag{21}$$

where $x_f^{\max}$ denotes the feedback location x_f associated with a maximum extractable work. We have verified the fact that $\partial^2\langle W\rangle/\partial x_f^2 > 0$ for $x_f = x_f^{\max}$ and for any positive values of G, a, and D. Therefore, Eq. (21) provides the best feedback location to obtain a maximum extractable work in this limit. The optimal choice of measurement and feedback positions that maximize $-\langle W\rangle_{\max}$ can be obtain by satisfying $\frac{\partial\langle W\rangle}{\partial x_m} = 0$ and $\frac{\partial\langle W\rangle}{\partial x_f} = 0$ simultaneously. The exact analytical condition in this limit reads

$$x_f^* = x_f^{\max}\big|_{x_m = x_m^*} \quad \text{and} \quad x_m^* = \frac{x_f^*}{2}, \tag{22}$$

where x_m^* and x_f^* denote the optimal value of measurement and feedback positions, respectively. Plugging them both into Eq. (21) results in a transcendental equation that can be solved numerically. The solution yields $x_m^* = 0.61\sigma$, where $\sigma = \sqrt{D/2Ga}$. Therefore, the observation agrees with the best extractable work restrictions reported earlier [21–23].

Similarly, under entropic dominance ($G/D \ll 1$), the average extractable work can be calculated as

$$\begin{aligned}-\langle W\rangle &= \frac{3}{4}\sqrt{\frac{a}{c^3}}\int_{-x_r+\Delta}^{x_r-\Delta} dx\,\omega(x)\ln\left(\frac{\omega(x-x_f)}{\omega(x)}\right)\\ &= T_1(x_m,x_f) + T_2(x_m,x_f) + T_3(x_m,x_f)\\ &\quad + T_4(x_m,x_f) + T_5(x_m,x_f),\end{aligned} \tag{23}$$

where

$$T_1(x_m,x_f) = \left(\frac{3}{4}\frac{x_f^2}{x_r^2} - \frac{1}{2}\right)\ln\left|\frac{(x_f+\Delta)(x_r - x_f + x_m)}{(2x_r + x_f - \Delta)(x_r + x_f - x_m)}\right|,$$

$$T_2(x_m,x_f) = -\frac{1}{2}\ln\left|\frac{2\Delta(x_r - x_f) + x_f x_r}{2x_r(2x_r - \Delta)}\right|,$$

$$T_3(x_m,x_f) = \frac{a^2 x_f}{4c\sqrt{c}}[(x_r - x_m)(2x_f - x_r + x_m) - 2\Delta(x_f - x_r)],$$

$$T_4(x_m,x_f) = \frac{1}{4}\frac{x_f^2}{x_r^3}\ln\left|\frac{a(x_f - x_r)^2 - 2a\Delta(x_f - x_r) - c}{a(x_f - x_m)^2 - c}\right|,$$

$$T_5(x_m,x_f) = x_m\left(\frac{1}{4}\frac{x_m^2}{x_r^2} - \frac{3}{4}\right)\ln\left|1 + \frac{a x_f(2x_m - x_f)}{c - a x_m^2}\right|.$$

Here, $|\cdots|$ denotes the absolute value of the observable. One can derive $x_f^{\max}$ theoretically following a similar method explained for the energy-dominated case. For a given x_m, the corresponding $x_f^{\max}$ will be the solution of the following transcendental equation (with $x_f = x_f^{\max}$):

$$\Theta_1(x_f) + \Theta_2(x_f) + \Theta_3(x_f) = 0,$$

$$\Theta_1(x_f) = -x_f x_r \ln\left|\frac{a x_f[a(x_m - x_f) + \sqrt{ac}]}{(2\sqrt{ac} - a x_f)[a(x_m - x_f) - \sqrt{ac}]}\right|,$$

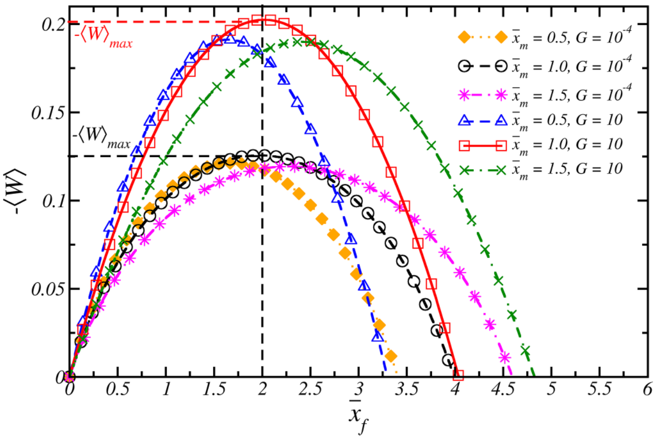

FIG. 5. Variation of average extractable work ($-\langle W\rangle$) with the scaled feedback position ($\bar{x}_f$) for different values of scaled measurement length ($\bar{x}_m$). Orange solid diamond, black circle, and magenta starred points are associated with $\bar{x}_m = 0.5,\ 1.0$, and 1.5, respectively, in a low-G limit ($G = 10^{-4}$). Blue triangle, red square, and green cross points are associated with $\bar{x}_m = 0.5,\ 1.0$, and 1.5, respectively, in an energy-dominated condition ($G = 10$). The parameter set chosen is $D = 1$, $a = 0.1$, and $c = 1.6$ for all cases.

$$\Theta_2(x_f) = \frac{1}{2}(x_m - x_r)(x_m + x_r + 2x_f),$$
$$\Theta_3(x_f) = \frac{-x_f^2}{2}\ln\left|\frac{2x_f\sqrt{ac} - ax_f^2}{ax_m^2 - 2ax_fx_m + ax_f^2 - c}\right|. \tag{24}$$

From Eqs. (23) and (24), one obtains the best extractable work requirement as $x_f^* = x_f^{\max}|_{x_m = x_m^*}$ and $x_m^* = \frac{x_f^*}{2}$. The condition yields

$$2x_m^*\ln\left|\frac{-ax_m^{*^2} + c}{4x_m^*(-ax_m^* + \sqrt{ac})}\right| + 2x_m^*x_r\ln\left|1 + \frac{x_r^2}{x_m^*}\right|$$
$$+ \frac{1}{2}(x_m^* - x_r)(5x_m^* + x_r) = 0. \tag{25}$$

Solution of the transcendental equation (25) gives the best recipe as $x_m^* = 0.6\sigma$ and $x_f^* = 2x_m^*$, where the standard deviation in this limit reads $\sigma = \sqrt{c/5a}$.

We find that for $G = 10$, the maximum extractable work is obtained when $x_m \approx 0.42$ and $x_f \approx 0.84$, and $\sigma \approx 0.71$. In the limit of $G \to 0$, $x_m \approx 1.07$ and $x_f \approx 2.14$, with $\sigma \approx 1.79$, provide the optimal condition for maximum extractable work. Therefore, despite the differences in dominance of G, the recipe to obtain maximum extractable work remains the same as $x_m = 0.6\sigma$ and $x_f = 2x_m$. We revisit the variation of the average extractable work per cycle $-\langle W\rangle$ as a function of a scaled position of the shifted confinement $\bar{x}_f$ for a different scaled measurement distance $\bar{x}_m$ and G. Here, we define a scaled observable $\bar{R}$ as $\bar{R} = R/x_m^*$. Results are shown in Fig. 5.

Figure 5 clearly shows that $-\langle W\rangle_{\max}$ is maximum for $\bar{x}_f = 2$, irrespective of the values of G. We determine the $x_f^{\max}$ for a given x_m using Eqs. (21) and (24) in respective limits of G. In this context, we mention that one can verify the aforementioned relation for any arbitrary values of G by estimating direct numerical integration of Eqs. (11), (12), (17), and (19). As mentioned earlier, Figs. 4 and 5 also show that the geometric trap can have extractable work ($-\langle W\rangle > 0$) only up to a certain value of the feedback position. The restriction $-\langle W\rangle = 0$ in Eq. (20) (under constant x_m) gives the upper bound of the feedback location as x_f^t. Using Eqs. (20) and (23), one can show that $x_f^t = 2x_f^{\max}$ invariant to the extent of entropic dominance.

To shine more light on these observations and to examine the differences of $-\langle W\rangle_{\max}$ between high and low values of G, we investigate the amount of total information ($\langle I\rangle$) and unavailable information ($\langle I_u\rangle$) during the feedback protocol. In the limit of $G/D \gg 1$, the net information acquired by the measurement can be estimated using Eqs. (13) and (18):

$$\langle I\rangle \simeq \frac{1}{2} - \ln\left(\sqrt{\frac{Ga}{\pi D}}\right). \tag{26}$$

Similarly, for the other extreme $G/D \ll 1$, the net information has the form [using Eqs. (14) and (18)]

$$\langle I\rangle \simeq \frac{5}{3} - \ln\left(3\sqrt{\frac{a}{c}}\right) \quad \text{in the limit of } \Delta \to 0. \tag{27}$$

For any arbitrary values of G, x_m, and x_f, using Eqs. (11)–(14) and Eqs. (17) and (18), one can show that

$$D(\langle I\rangle - \langle I_u\rangle) = -\langle W\rangle. \tag{28}$$

Equation (28) clearly shows that the available information during the feedback cycles coincides with the net change in the effective potential experienced by the particle during the feedback step. Here, we recall that the useful information ($\langle I\rangle - \langle I_u\rangle$) has been calculated in terms of marginal equilibrium probability distribution $P_{\rm eq}(x)$. One can obtain $P_{\rm eq}(x)$ numerically from the underlying 2D Langevin dynamics [Eqs. (1) and (2)]. On the other hand, the average work has been calculated using the effective potential energy change in the reduced dimension. Therefore, the effective description of system dynamics in reduced dimension can quantify the limit of extractable energy (say, work) using the available information associated with the feedback mechanism. In other words, analyzing the condition for best achievable work is equivalent to optimizing the utilization of available information.

Therefore, Eq. (28) signifies that for an instantaneous (error-free) measurement and feedback process, available information acquired during the protocol can, in principle, entirely be extracted as useful energy [21–23]. Popularly, such types of engines are denoted as lossless information engines [22]. Therefore, the GBIE can be considered as a lossless engine in the sense that it converts all the available information ($\langle I\rangle - \langle I_u\rangle$) into extractable work. In a true sense, however, it is not completely lossless. Because of the irreversible nature of the protocol, a finite amount of acquired information is lost during the relaxation phase. However, it is worthwhile to mention that one may design and introduce a reversible protocol in which the net acquired information is equivalent to available information ($\langle I_u\rangle = 0$) [88,89].

In Fig. 6, we study the variation of average information ($\langle I\rangle$) and unavailable information ($\langle I_u\rangle$) during the feedback with the scaled position of the shifted confinement center $\bar{x}_f$ for different values of $\bar{x}_m$. Results show that the total acquired information is independent of feedback position for a given system parameter set. However, the amount of unavailable

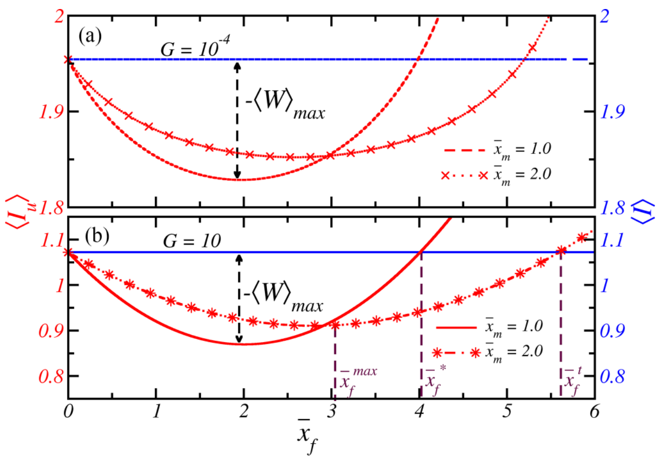

FIG. 6. Change in average information ($\langle I\rangle$) and unavailable information ($\langle I_u\rangle$) with increasing scaled feedback position $\bar{x}_f$ for different values of scaled measurement position ($\bar{x}_m$). Parameter set chosen: $D = 1$, $a = 0.1$, and $c = 1.6$ for all cases. Part (a) represents the variation in the entropy-dominated regime $G = 10^{-4}$. (b) The same in an energy-controlled situation $G = 10$.

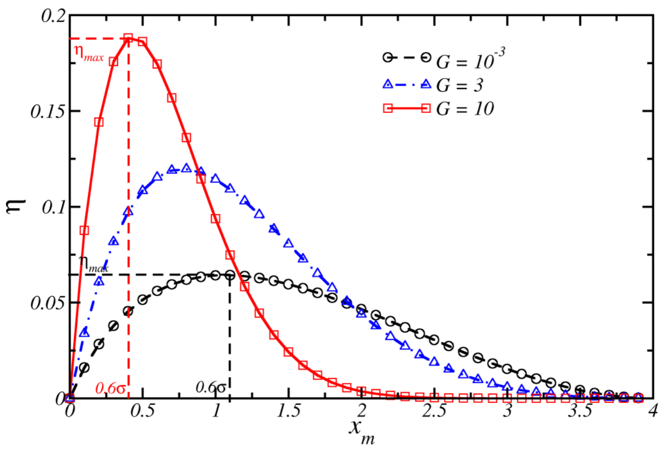

FIG. 7. Variation of the efficiency (η) with the measurement position (x_m) for a fixed feedback location ($x_f = 2x_m$) and different G. Parameter set chosen: $D = 1$, $a = 0.1$, and $c = 1.6$ for all cases.

information ($\langle I_u\rangle$) varies nonmonotonically with increasing x_f. In the limit of $x_f \to 0$, all the acquired information is lost during the relaxation process as there is no change in the effective potential of the system. Using Eqs. (13) and (14), one realizes $\langle I_u\rangle \simeq \langle I\rangle$ for $x_f \to 0$. With an increasing x_f, the distance between the measurement position and the feedback site decreases. Consequently, the number of singular paths decreases during relaxation, and particles reach the new potential minimum with less uncertainty. This results in a decrease in unavailable information. As a result, the amount of extractable work increases. At this stage, it is worthwhile to mention that the loss of acquired information during measurement happens because of the presence of *unusual* pathways (singular) during the relaxation process. For the protocol with error-free measurement, a measured outcome is greater (or lesser) than x_m if and only if the particle resides in the $x > x_m$ (or $x < x_m$) region. We then employ the feedback based on the measurement outcome and allow the system to relax. However, after the relaxation stage, particles can reside in the $x > x_m$ (or $x < x_m$) region even though the measured outcome was greater (or lesser) than x_m. We denote these relaxation pathways as singular paths; the measurement of such paths contributes to information lost during the process. For a better understanding of singular paths and their contribution in determining $\langle I_u\rangle$, we refer to Szilard's engine as discussed in [14].

Coming back to Fig. 6, for $x_f \gg x_m$, $\langle I_u\rangle > \langle I\rangle$ as the contribution of the second term of the right-hand side of Eq. (14) dominates. The situation corresponds to a large shift in the detention center (hence the effective potential). The distance between x_m and x_f becomes large again. Thus, the number of singular paths during the relaxation processes increases again, resulting in a decrease in the magnitude of $\langle W\rangle$ due to the heavy information loss during relaxation. Therefore, one optimum x_f distance exists where the loss of information is minimum, and the condition corresponds to the recipe of maximum extractable work. For a given protocol, the $\langle I\rangle$ is invariant to the feedback position [see Eqs. (13), (26), and (27)]. Therefore, the relation Eq. (28) suggests that the condition for a minimum $\langle I_u\rangle$ is identical to the optimal recipe of maximum achievable work.

The argument promotes the existence of a nonzero x_f^t for which total information levels the loss due to the relaxation process. Beyond this point, the protocol results in refrigeration ($-\langle W\rangle < 0$). Finally, Fig. 6 also shows that both the information and unavailable information increase for decreasing G. However, in the low-G limit, the rise in unavailable information is relatively higher than the total information. Consequently, one can witness that the amount of maximum extractable $-\langle W\rangle_{\max}$ at optimal measurement distance x_m^* is higher in the energy-ruled region than that of the entropic case.

Next, we calculate the efficiency of the information engine, which can be defined as $\eta = -\langle W\rangle/D\langle I\rangle$. In Fig. 7, we study the variation of efficiency (η) with the measurement distance (x_m) for the protocol with a feedback site twice as large as the measurement distance ($x_f = 2x_m$). Results show that the engine efficiency varies nonmonotonically with the measurement distance (x_m). The variation depicts that the engine's efficiency is always less than unity, and it has a maximum at the measurement distance $\approx 0.6\sigma$ (σ is the standard deviation) irrespective of the magnitude of the transverse force. As the efficiency cannot reach unity, the engine is not a completely lossless one. Also, the engine is most efficient when unavailable information is minimal during the employed feedback process. Figure 7 shows that $\eta_{\max}$ decreases with higher entropic control of the system. This reduction in $\eta_{\max}$ can be attributed to the lower achievable work and the increase in the available information in the low-G limit.

Finally, one can find that the present setup is consonant with the integral fluctuation theorem [14]:

$$\left\langle \exp\left(-\frac{W_d}{D} - I + I_u\right)\right\rangle = \int_{-x_r}^{x_m} dx\, P_{\rm eq}(x) + \int_{x_m}^{x_r} dx\, P_{\rm eq}(x) \times \exp\left(\frac{A(x) - A(x - x_f)}{D}\right) \frac{P_{\rm eq}(x)}{P_{\rm eq}(x - x_f)} = 1. \quad (29)$$

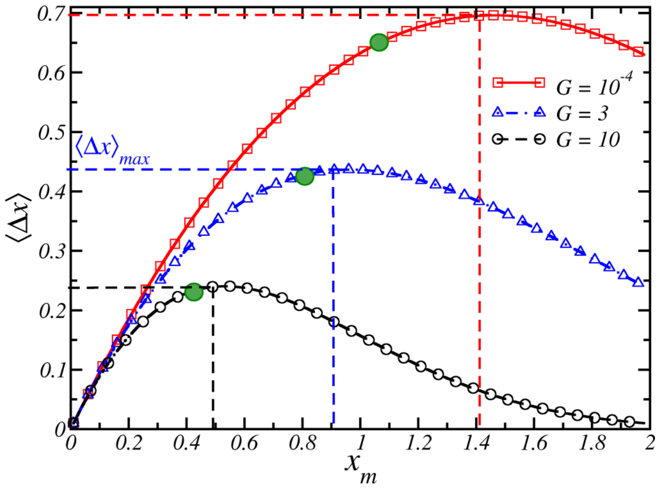

FIG. 8. Variation of the average unidirectional step per cycle ($\langle\Delta x\rangle$) observed during the feedback protocol with the measurement position (x_m) for different values of downwards bias force (G). Parameter set chosen: $x_f = 2x_m$, $D = 1$, $a = 0.1$, and $c = 1.6$ for all cases. Green filled circles indicate the $\langle\Delta x\rangle$ associated with the best extractable work extraction condition ($x_m^* \sim 0.6\sigma$).

We estimated the dissipated energy as $W_d = A(x - x_f) - A(x)$.

C. Optimization of average displacement $\langle\Delta x\rangle$ and efficacy (γ)

The average displacement per cycle ($\langle\Delta x\rangle$) measures the mean unidirectional motion of particles during the feedback mechanism. Therefore, $\langle\Delta x\rangle$ quantifies unidirectional transport induced by the information engine that operates in a single heat bath. For an irrational choice of the transverse bias force (G), we obtain $\langle\Delta x\rangle$ using Eqs. (16), and (17). The definition of $\langle\Delta x\rangle$ [Eq. (16)] clearly shows that it varies linearly with respect to the feedback position (x_f). Inspired by the observation of the previous subsection, one can assume that a good feedback location depends on the choice of the measurement distance. Therefore, we consider a fixed feedback distance, as a double of the measurement position $x_f = 2x_m$, and we examine the response of $\langle\Delta x\rangle$ for different x_m. Figure 8 shows the variation of $\langle\Delta x\rangle$ as a function of the measurement position (x_m) for different entropic control. The variations depict a turnover in $\langle\Delta x\rangle$ with increasing x_m. Equation (16) under the constraint of $x_f = 2x_m$ indicates a tradeoff between the x_m and integrated marginal probability $[P(x,t)]$ of particles beyond x_m in determining $\langle\Delta x\rangle$. To obtain a quantitative measure of the optimal control on $\langle\Delta x\rangle$, we recall Eqs. (16) and (18) and examine the limiting responses. Under the restriction of $x_f = 2x_m$, we find

$$\begin{aligned}\langle\Delta x\rangle &= x_m \mathrm{erfc}\left(\sqrt{\frac{Ga}{D}}x_m\right) \qquad \text{for } \frac{G}{D} \gg 1\\ &= x_m - \frac{3}{2}\sqrt{\frac{a}{c}}x_m^2 + \frac{1}{2}\sqrt{\frac{a^3}{c^3}}x_m^4 \quad \text{for } \frac{G}{D} \ll 1. \qquad (30)\end{aligned}$$

Thus, in both ends of G, $\langle\Delta x\rangle$ varies nonmonotonically with x_m. This drives the manifestation of an optimum measurement distance to accomplish the largest average displacement per cycle.

Figure 8 also reveals that both the best average distance $\langle\Delta x\rangle_{\max}$ and the concerned measurement distance increase by introducing more entropic control to the process. One can determine the optimum value of x_m for achieving maximum $\langle\Delta x\rangle$ by maximizing Eq. (30). For a high G, $\frac{\partial\langle\Delta x\rangle}{\partial x_m} = 0$ yields

$$x_m = \sqrt{\frac{\pi}{2}}\sigma\, \mathrm{erfc}\left(\frac{x_m}{\sqrt{2}\sigma}\right)\exp\left(\frac{-x_m^2}{2\sigma^2}\right). \qquad (31)$$

Numerical solution of this transcendental equation gives $x_m = 0.75\sigma$, where $\sigma = \sqrt{D/2Ga}$. For $G \to 0$, the restriction $\frac{\partial\langle\Delta x\rangle}{\partial x_m} = 0$ results in

$$1 - \frac{3}{\sqrt{5}}\frac{x_m}{\sigma} + \frac{2}{5\sqrt{5}}\frac{x_m^3}{\sigma^3} = 0. \qquad (32)$$

The solution of the cubic polynomial gives the measurement position related to the best average displacement as 0.81σ, where the standard deviation $\sigma = \sqrt{c/5a}$ for this case. Finally, it is noteworthy that the requirement to have a maximum $\langle\Delta x\rangle$ is not identical to the best extractable work condition. Using these restrictions, we find the best average displacement $\langle\Delta x\rangle \approx 0.24$ and ≈ 0.70 for $G = 10$ and 10^{-4}, respectively. Therefore, the maximum average displacement per cycle is higher under an entropic control than in the energy-governed setup. One can explain the enhanced value of $\langle\Delta x\rangle_{\max}$ for a purely entropic information engine in terms of the shape of the equilibrium probability distribution. In the limit of $G \to 0$, the $P_{\mathrm{eq}}(x)$ has an inverted parabola-like outline along the feedback coordinate (Fig. 3). This increases the standard deviation of the distribution in comparison to the $P_{\mathrm{eq}}(x)$ with high transverse bias. Consequently, the marginal probability towards the confinement terminus ($x_m < x < x_r$) is higher under entropic control. Therefore, the integrated probability of particles crossing a high measurement distance is higher. This results in high $\langle\Delta x\rangle$ in a purely entropic GBIE.

Finally, we study the hallmarks of the efficacy of the feedback controller of a GBIE using Eq. (15) under the condition of $x_f = 2x_m$. The results are shown in Fig. 9. The following observations are evident. The efficacy (γ) varies nonmonotonically with increasing measurement position. The efficacy approaches unity, $\gamma = 1$, for both extremes of the measurement distances, i.e., either $x_m = 0$ or $x_m \to x_r$ for all three different values of transverse force G. The magnitude of the maximum efficacy $\gamma \approx 1.9$ is higher for $G = 10$, whereas it is less for $G = 10^{-4}$, $\gamma \approx 1.22$. The corresponding measurement position to maximum efficacy is obtained at $x_m \approx 1.33$, invariant in G. Thus, the recipe to obtain $\gamma_{\max}$ differs from the best extractable work prescription.

Using Eqs. (15) and (18), the efficacy of the process under energetic and entropic extremes takes the form

$$\begin{aligned}\gamma = \frac{1}{2} + \frac{1}{2}\Bigg[&\mathrm{erf}\left(\sqrt{\frac{Ga}{D}}x_m\right) - \mathrm{erf}\left(\sqrt{\frac{Ga}{D}}(x_m - x_f)\right)\\ &+ \mathrm{erf}\left(\sqrt{\frac{Ga}{D}}(x_r - x_f)\right)\Bigg] \qquad (33)\end{aligned}$$

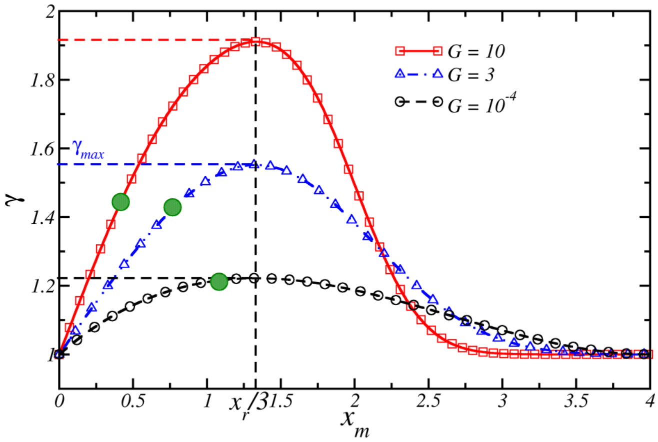

FIG. 9. Variation of the efficacy of the feedback protocol (γ) with the measurement position (x_m) for different G. Parameter set chosen: $x_f = 2x_m$, $D = 1$, $a = 0.1$, and $c = 1.6$ for all cases. Green filled circles indicate the efficacy associated with the best extractable work condition ($x_m^* \sim 0.6\sigma$).

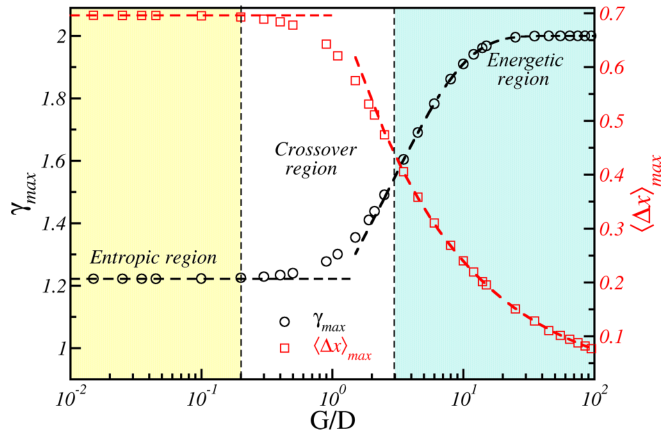

FIG. 10. Variation of the best efficacy ($\gamma_{\max}$) and the best displacement per cycle $\langle \Delta x\rangle_{\max}$ with transverse force (G/D). Parameter set chosen: $x_f = 2x_m$, $D = 1$, $a = 0.1$, and $c = 1.6$ for all cases. Points are obtained by the numerical integration of the general expressions of efficacy [Eq. (15)] and averaged distance per cycle [Eq. (16)] under the restriction of $x_f = 2x_m$. Dashed lines are obtained from the theoretical expressions related to the limiting behavior.

and

$$\gamma = 1 + \frac{3}{4}\sqrt{\frac{a^3}{c^3}}x_f(x_r - x_m)(x_r + x_m - x_f), \tag{34}$$

respectively. In either case, the efficacy of the engine, under the constraint $x_f = 2x_m$, reduces to a univariate function of x_m. In the limit of $G/D \gg 1$, Eq. (33) reduces to

$$\gamma = \frac{1}{2} + \mathrm{erf}\left(\sqrt{\frac{Ga}{D}}x_m\right) + \frac{1}{2}\mathrm{erf}\left(\sqrt{\frac{Ga}{D}}(x_r - 2x_m)\right). \tag{35}$$

On the other hand, the restriction $x_f = 2x_m$ reduces Eq. (34) to

$$\gamma = 1 + \frac{3}{4}\sqrt{\frac{a^3}{c^3}}2x_m(x_r - x_m)^2. \tag{36}$$

From, Eqs. (35) and (36), it is obvious that γ converges to unity for either extreme of the measurement positions, $x_m = 0$ and $x_m \to x_r$, irrespective to the strength of the transverse force. Also, as expressed in Eqs. (35) and (36), γ varies nonmonotonically with x_m. We find that the best value of x_m that generates maximum efficacy is $\frac{x_r}{3}$ in either case and is independent of G and any other geometric parameter. Finally, using the condition $x_m = \frac{x_r}{3}$ on Eqs. (35) and (36), one can find that $\gamma \to 2$ in the limit of $G/D \gg 1$, whereas $\gamma = \frac{11}{9}$ in the other extreme. As mentioned earlier, the spread of the marginal probability distribution is broader in an entropy-dominated situation, and hence the particles can relax in a higher number of paths. Therefore, the protocol's efficacy reduces compared to an energetic system. To summarize the subsection, we depict that both $\langle \Delta x\rangle_{\max}$ and $\gamma_{\max}$ show a crossover response once the system is driven from an entropic to an energetic-dominated regime, as shown in Fig. 10.

Before we conclude, we mention a few pertinent observations on the experimental feasibility of a GBIE. First, the setup requires a Brownian diffusion inside a narrow channel with irregular geometry and suitable measurement techniques that can relate the underlying available information to the thermodynamic outputs. A recent experiment on diffusion through a corrugated channel by Yang *et al.* demonstrates an entropy-driven transport [90]. They have fabricated irregular channels using a two-photon writing system followed by the imaging procedure, and they studied the diffusion of fluorescently labeled polystyrene colloidal particles inside the cavity. Furthermore, the study also validates the Fick-Jacobs approximation once the hydrodynamics effects are considered. In another investigation, researchers studied the entropic ratcheting effect due to channel asymmetry [91]. One can microfabricate a narrow channel using photolithography [91]. The diffusion of colloids across a constrained geometry has been studied using microfluidics and holographic optical tweezers [92,93]. On the other hand, recent experimental developments illustrate the design principle of different Brownian information engines [20,22–26]. These studies display the interconversion between the information and other thermodynamic outcomes. Therefore, one can map the entropic constraints by designing a suitable narrow cavity in the spirit of [90–93], and one can measure the thermodynamic observable (from available information) introducing feedback procedures employed in [20,22–26]. The outcome of the current study, therefore, orchestrates a perfect standard to devise such geometric information engines.

Second, the net change in the effective potential is equivalent to the change in free energy of the particle during the feedback process. However, it is tricky to demonstrate work extraction physically. This is because the present GBIE setup does not have a suitable force, in the 2D Langevin process, along the feedback direction that defines a work. The presence of such a force would be helpful to verify its crosstalk to the effective entropic potential [$A(x)$] and hence to the information ($\langle I\rangle$). One way to verify the utilization of available information is to consider a weak external force along the negative feedback direction. One can now calculate the work done in the presence of the applied force and compare the same with the available information acquired. The difference will be reflected in the change in the average step per cycle.

Finally, the effect of the irregular boundaries and hence the effective entropic potential in reduced dimension on the stochastic energetic of the system can also be understood as follows. Consider the motion of Brownian particles inside a two-dimensional enclosure in the presence of a time-periodic field that acts upon the particle along the longitudinal direction. One can obtain the work done over a cycle and its fluctuations from the original 2D Langevin description. A finite nonzero work is obtained inside such constrained geometry by appropriate manipulation of the external periodic driving frequency and noise strength. $\langle W \rangle$ shows a maximum for optimal noise strength [96]. Therefore, $\langle W \rangle$ is a suitable quantifier for an entropic stochastic resonance (SR) phenomenon [44,64,94–96]. It is important to notice that although there was no nonlinear potential (crucial criteria for SR to be observed [94,95]) in the original dynamics, the bistability in the effective entropic potential [$A(x)$] satisfies the requirement [44,64,96]. Therefore, $A(x)$ obtained from the Fick-Jacobs approximation in reduced dimension is feasible in describing the energetic of the system under the appropriate setup.

IV. CONCLUSIONS

We explore the optimum operating condition of a GBIE built of Brownian particles trapped in monostable confinement and subjected to error-free feedback regulation. The cycles utilize the information gathered for extractable work and submit a unidirectional passage of the particle. The upshots of the measurement position x_m and the feedback site x_f circumscribe the engine's performance. We determine the optimal condition for maximizing the extractable work ($-\langle W \rangle$), the average displacement per cycle ($\langle \Delta x \rangle$), and the effectiveness of the protocol (γ) under varying entropic authority.

Analogous to other Brownian information engines [21–23], the GBIE under a feedback controller can completely utilize the available information and hence be regarded as a lossless information engine. We specify the criteria for utilizing the available information in an output extractable work and the optimum operating requisites for the best extractable work. The maximum extractable work is possible when $x_m = 0.6\sigma$ and $x_f = 2x_m$. The observation is consonant with the best extractable work restrictions reported earlier [21–23] and showed the universality of requisites. Nonetheless, the measurement distance and feedback site positions alter upon remodeling of entropic dominance as the standard deviation itself develops during such parameter tuning. In an energy-dominated process, σ depends on the ratio of the thermal energy to the advective energy of the process as $\sigma = \sqrt{D/2Ga}$. On the other hand, σ becomes independent of G and depends only on the geometric aspect ratio ($x_r = \sqrt{c/a}$) in a purely entropic control. The magnitude of the extractable work grows with increasing transverse force G. One can justify the lower benefits of achievable work in an entropy-ruled scenario in terms of the elevated loss in information during the relaxation process.

Next, we find the condition on x_m for maximum average displacement per cycle ($\langle \Delta x \rangle$) with a restriction on the feedback site as $x_f = 2x_m$. The measurement position that gives the best average displacement varies with the extent of entropic control. For high G values ($\gg 1$), we find $x_m \sim 0.75\sigma$, and in the limit of $G \to 0$, the $x_m \sim 0.81\sigma$ is responsible for best unidirectional motion ($\langle \Delta x \rangle_{\max}$). Therefore, unlike the extractable work, the mean unidirectional displacement of particles is higher in the entropy-dominated regime than in the energy-governed system. Upon decreasing G, the spread of the equilibrium marginal probability distribution [$P_{\text{eq}}(x)$] becomes wider (higher σ). Consequently, a bigger fraction of particles can satisfy the measurement requirement, which increases the $\langle \Delta x \rangle_{\max}$ value in an entropically driven system.

Finally, under a given feedback location $x_f = 2x_m$, the maximum efficacy ($\gamma_{\max}$) is invariant with the transverse force strength G and achieved when $x_m = x_r/3$. $\gamma_{\max}$ approaches the universal upper bound 2 under firm energetic control. Upon lowering down the energetic power, the upper bound becomes tighter and shows a crossover to $\gamma_{\max} = \frac{11}{9}$ for a purely entropic device. We trust that the outcomes of the present study will help to design geometric information engines and will result in new avenues for further theoretical and experimental investigations.

ACKNOWLEDGMENTS

R.R. and S.Y.A. acknowledge IIT Tirupati for a fellowship. D.M. thanks SERB (Project No. ECR/2018/002830/CS), Department of Science and Technology, Government of India, for financial support, and IIT Tirupati for the new faculty seed grant.

The authors have no conflicts to disclose.

[1] H. S. Leff and A. F. Rex, *Maxwell's Demon 2: Entropy, Classical and Quantum Information, Computing* (Princeton University Press, Princeton, NJ, 2003).

[2] A. F. Rex, Maxwell's demon—A historical review, Entropy **19**, 240 (2017).

[3] R. Landauer, Irreversibility and heat generation in the computing process, IBM J. Res. Dev. **5**, 183 (1961).

[4] C. H. Bennet, The thermodynamics of computation—A review, Int. J. Theor. Phys. **21**, 905 (1982).

[5] L. Brillouin, Maxwell's demon cannot operate: Information and entropy. I, J. Appl. Phys. **22**, 334 (1951).

[6] L. Szilard, Über die Entropieverminderung in einem thermodynamischen System bei Eingriffen intelligenter wesen, Z. Phys. **53**, 840 (1929).

[7] T. Sagawa and M. Ueda, Second Law of Thermodynamics with Discrete Quantum Feedback Control, Phys. Rev. Lett. **100**, 080403 (2008).

[8] T. Sagawa and M. Ueda, Minimal Energy Cost for Thermodynamic Information Processing: Measurement and Information Erasure, Phys. Rev. Lett. **102**, 250602 (2009).

[9] T. Sagawa and M. Ueda, Generalized Jarzynski Equality under Nonequilibrium Feedback Control, Phys. Rev. Lett. **104**, 090602 (2010).

[10] C. Jarzynski, Nonequilibrium Equality for Free Energy Differences, Phys. Rev. Lett. **78**, 2690 (1997).

[11] J. M. Horowitz and S. Vaikuntanathan, Nonequilibrium detailed fluctuation theorem for repeated discrete feedback, Phys. Rev. E **82**, 061120 (2010).

[12] D. Abreu and U. Seifert, Extracting work from a single heat bath through feedback, Europhys. Lett. **94**, 10001 (2011).
[13] P. S. Pal, S. Rana, A. Saha, and A. M. Jayannavar, Extracting work from a single heat bath: A case study of a Brownian particle under an external magnetic field in the presence of information, Phys. Rev. E **90**, 022143 (2014).
[14] Y. Ashida, K. Funo, Y. Murashita, and M. Ueda, General achievable bound of extractable work under feedback control, Phys. Rev. E **90**, 052125 (2014).
[15] S. W. Kim, T. Sagawa, S. De Liberato, and M. Ueda, Quantum Szilard Engine, Phys. Rev. Lett. **106**, 070401 (2011).
[16] D. E. Bruschi, M. Perarnau-Llobet, N. Friis, K. V. Hovhannisyan, and M. Huber, Thermodynamics of creating correlations: Limitations and optimal protocols, Phys. Rev. E **91**, 032118 (2015).
[17] J. Goold, M. Huber, A. Riera, L. Del Rio, and P. Skrzypczyk, The role of quantum information in thermodynamics—A topical review, J. Phys. A **49**, 143001 (2016).
[18] B. J. Lopez, N. J. Kuwada, E. M. Craig, B. R. Long, and H. Linke, Realization of a Feedback Controlled Flashing Ratchet, Phys. Rev. Lett. **101**, 220601 (2008).
[19] S. Toyabe, T. Sagawa, M. Ueda, E. Muneyuki, and M. Sano, Experimental demonstration of information-to-energy conversion and validation of the generalized Jarzynski equality, Nat. Phys. **6**, 988 (2010).
[20] A. Bérut, A. Arakelyan, A. Petrosyan, S. Ciliberto, R. Dillenschneider, and E. Lutz, Experimental verification of Landauer principle linking information and thermodynamics, Nature (London) **483**, 187 (2012).
[21] J. M. Park, J. S. Lee, and J. D. Noh, Optimal tuning of a confined Brownian information engine, Phys. Rev. E **93**, 032146 (2016).
[22] G. Paneru, D. Y. Lee, T. Tlusty, and H. K. Pak, Lossless Brownian Information Engine, Phys. Rev. Lett. **120**, 020601 (2018).
[23] G. Paneru, D. Y. Lee, J. M. Park, J. T. Park, J. D. Noh, and H. K. Pak, Optimal tuning of a Brownian information engine operating in a nonequilibrium steady state, Phys. Rev. E **98**, 052119 (2018).
[24] G. Paneru and H. K. Pak, Colloidal engines for innovative tests of information thermodynamics, Adv. Phys. X **5**, 1823880 (2020).
[25] S. Dago, J. Pereda, N. Barros, S. Ciliberto, and L. Bellon, Information and Thermodynamics: Fast and Precise Approach to Landauer's Bound in an Underdamped Micromechanical Oscillator, Phys. Rev. Lett. **126**, 170601 (2021).
[26] G. Paneru, S. Dutta, T. Sagawa, T. Tlusty, and H. K. Pak, Efficiency fluctuations and noise induced refrigerator-to-heater transition in information engines, Nat. Commun. **11**, 1012 (2020).
[27] V. Blickle and C. Bechinger, Realization of a micrometre-sized stochastic heat engine, Nat. Phys. **8**, 143 (2012).
[28] A. Kumari, P. S. Pal, A. Saha, and S. Lahiri, Stochastic heat engine using an active particle, Phys. Rev. E **101**, 032109 (2020).
[29] V. Holubec and R. Marathe, Underdamped active Brownian heat engine, Phys. Rev. E **102**, 060101(R) (2020).
[30] R. Zakine, A. Solon, T. Gingrich, and F. Van Wijland, Stochastic stirling engine operating in contact with active baths, Entropy **19**, 193 (2017).
[31] J. R. Gomez-Solano, Work extraction and performance of colloidal heat engines in viscoelastic baths, Front. Phys. **9**, 643333 (2021).
[32] I. A. Martínez, É. Roldán, L. Dinis, D. Petrov, J. M. Parrondo, and R. A. Rica, Brownian Carnot engine, Nat. Phys. **12**, 67 (2016).
[33] T. K. Saha, J. N. E. Lucero, J. Ehrich, D. A. Sivak, and J. Bechhoefer, Maximizing power and velocity of an information engine, Proc. Natl. Acad. Sci. USA **118**, e2023356118 (2021).
[34] D. Chiuchiù, M. López-Suárez, I. Neri, M. C. Diamantini, and L. Gammaitoni, Cost of remembering a bit of information, Phys. Rev. A **97**, 052108 (2018).
[35] D. Chiuchiú, M. C. Diamantini, and L. Gammaitoni, Conditional entropy and Landauer principle, Europhys. Lett. **111**, 40004 (2015).
[36] J. V. Koski, V. F. Maisi, J. P. Pekola, and D. V. Averin, Experimental realization of a Szilard engine with a single electron, Proc. Natl. Acad. Sci. USA **111**, 13786 (2014).
[37] K. Proesmans, J. Ehrich, and J. Bechhoefer, Finite-Time Landauer Principle, Phys. Rev. Lett. **125**, 100602 (2020).
[38] K. Proesmans, J. Ehrich, and J. Bechhoefer, Optimal finite-time bit erasure under full control, Phys. Rev. E **102**, 032105 (2020).
[39] S. Y. Ali, R. Rafeek, and D. Mondal, Geometric information engine: Upper bound of extractable work under feedback control, J. Chem. Phys. **156**, 014902 (2022).
[40] R. Zwanzig, Diffusion past an entropy barrier, J. Phys. Chem. **96**, 3926 (1992).
[41] D. Reguera and J. Rubi, Kinetic equations for diffusion in the presence of entropic barriers, Phys. Rev. E **64**, 061106 (2001).
[42] D. Reguera, G. Schmid, P. S. Burada, J. M. Rubí, P. Reimann, and P. Hänggi, Entropic Transport: Kinetics, Scaling, and Control Mechanisms, Phys. Rev. Lett. **96**, 130603 (2006).
[43] P. S. Burada, G. Schmid, D. Reguera, J. Rubi, and P. Hänggi, Biased diffusion in confined media: Test of the Fick-Jacobs approximation and validity criteria, Phys. Rev. E **75**, 051111 (2007).
[44] P. S. Burada, G. Schmid, D. Reguera, M. H. Vainstein, J. M. Rubi, and P. Hänggi, Entropic Stochastic Resonance, Phys. Rev. Lett. **101**, 130602 (2008).
[45] P. S. Burada, G. Schmid, D. Reguera, J. Rubi, and P. Hänggi, Entropic stochastic resonance: The constructive role of the unevenness, Eur. Phys. J. B **69**, 11 (2009).
[46] D. Mondal and D. S. Ray, Diffusion over an entropic barrier: Non-Arrhenius behavior, Phys. Rev. E **82**, 032103 (2010).
[47] B. Q. Ai and L. G. Liu, A channel Brownian pump powered by an unbiased external force, J. Chem. Phys. **128**, 024706 (2008).
[48] D. Mondal, M. Das, and D. S. Ray, Entropic noise-induced nonequilibrium transition, J. Chem. Phys. **133**, 204102 (2010).
[49] P. Kalinay and J. Percus, Projection of two-dimensional diffusion in a narrow channel onto the longitudinal dimension, J. Chem. Phys. **122**, 204701 (2005).
[50] D. Mondal, M. Das, and D. S. Ray, Entropic dynamical hysteresis in a driven system, Phys. Rev. E **85**, 031128 (2012).
[51] D. Mondal, M. Das, and D. S. Ray, Entropic resonant activation, J. Chem. Phys. **132**, 224102 (2010).
[52] P. S. Burada, G. Schmid, P. Talkner, P. Hänggi, D. Reguera, and J. M. Rubí, Entropic particle transport in periodic channels, Biosystems **93**, 16 (2008).
[53] M. Das, D. Mondal, and D. S. Ray, Shape fluctuation-induced dynamic hysteresis, J. Chem. Phys. **136**, 114104 (2012).

[54] D. Mondal and D. S. Ray, Asymmetric stochastic localization in geometry controlled kinetics, J. Chem. Phys. **135**, 194111 (2011).
[55] P. S. Burada, G. Schmid, D. Reguera, J. M. Rubi, and P. Hänggi, Double entropic stochastic resonance, Europhys. Lett. **87**, 50003 (2009).
[56] M. Das, D. Mondal, and D. S. Ray, Logic gates for entropic transport, Phys. Rev. E **86**, 041112 (2012).
[57] M. Das, D. Mondal, and D. S. Ray, Shape change as entropic phase transition: A study using Jarzynski relation, J. Chem. Sci. **124**, 21 (2012).
[58] M. Das, Entropic memory erasure, Phys. Rev. E **89**, 032130 (2014).
[59] P. Malgaretti, M. Janssen, I. Pagonabarraga, and J. M. Rubi, Driving an electrolyte through a corrugated nanopore, J. Chem. Phys. **151**, 084902 (2019).
[60] A. Arango-Restrepo and J. M. Rubi, Entropic transport in a crowded medium, J. Chem. Phys. **153**, 034108 (2020).
[61] H. X. Zhou, Diffusion-influenced transport of ions across a transmembrane channel with an internal binding site, J. Phys. Chem. Lett. **1**, 1973 (2010).
[62] M. Muthukumar, Polymer escape through a nanopore, J. Chem. Phys. **118**, 5174 (2003).
[63] D. Mondal and M. Muthukumar, Ratchet rectification effect on the translocation of a flexible poly electrolyte chain, J. Chem. Phys. **145**, 084906 (2016).
[64] D. Mondal and M. Muthukumar, Stochastic resonance during a polymer trans location process, J. Chem. Phys. **144**, 144901 (2016).
[65] H. X. Zhou and R. Zwanzig, A rate process with an entropy barrier, J. Chem. Phys. **94**, 6147 (1991).
[66] T. Guérin, M. Dolgushev, O. Bénichou, and R. Voituriez, Universal kinetics of imperfect reactions in confinement. Commun. Chem. **4**, 157 (2021).
[67] D. A. Kessler and E. Barkai, Theory of Fractional Lévy Kinetics for Cold Atoms Diffusing in Optical Lattices, Phys. Rev. Lett. **108**, 230602 (2012).
[68] D. A. Kessler and E. Barkai, Infinite Covariant Density for Diffusion in Logarithmic Potentials and Optical Lattices, Phys. Rev. Lett. **105**, 120602 (2010).
[69] E. Lutz and F. Renzoni, Beyond Boltzmann–Gibbs statistical mechanics in optical lattices, Nat. Phys. **9**, 615 (2013).
[70] A. Dechant, E. Lutz, D. Kessler, and E. Barkai, Fluctuations of Time Averages for Langevin Dynamics in a Binding Force Field, Phys. Rev. Lett. **107**, 240603 (2011).
[71] D. Poland and H. A. Scheraga, Phase transitions in one dimension and the Helix—Coil transition in polyamino acids, J. Chem. Phys. **45**, 1456 (1966).
[72] D. Poland and H. A. Scheraga, Occurrence of a phase transition in nucleic acid models, J. Chem. Phys. **45**, 1464 (1966).
[73] A. Bar, Y. Kafri, and D. Mukamel, Loop Dynamics in DNA Denaturation, Phys. Rev. Lett. **98**, 038103 (2007).
[74] V. Kaiser and T. Novotný, Loop exponent in DNA bubble dynamics, J. Phys. A **47**, 315003 (2014).
[75] H. C. Fogedby and R. Metzler, DNA Bubble Dynamics as a Quantum Coulomb Problem, Phys. Rev. Lett. **98**, 070601 (2007).
[76] F. J. Dyson, A Brownian-motion model for the eigenvalues of a random matrix, J. Math. Phys. **3**, 1191 (1962).
[77] G. S. Manning, Limiting laws and counterion condensation in polyelectrolyte solutions I. Colligative properties, J. Chem. Phys. **51**, 924 (1969).
[78] H. Spohn, Tracer dynamics in Dyson's model of interacting Brownian particles, J. Stat. Phys. **47**, 669 (1987).
[79] P. H. Chavanis, C. Rosier, and C. Sire, Thermodynamics of self-gravitating systems, Phys. Rev. E **66**, 036105 (2002).
[80] E. Levine, D. Mukamel, and G. Schütz, Zero-range process with open boundaries, J. Stat. Phys. **120**, 759 (2005).
[81] S. Ray and S. Reuveni, Diffusion with resetting in a logarithmic potential, J. Chem. Phys. **152**, 234110 (2020).
[82] C. W. Gardiner, *Handbook of Stochastic Methods* (Springer, New York, 2003).
[83] D. R. Cox and H. D. Miller, *The Theory of Stochastic Processes* (CRC Press, Boca Raton, FL, 2001).
[84] H. Risken, *The Fokker-Planck Equation: Methods of Solution and Applications* (Springer-Verlag, Berlin, Heidelberg, 1989).
[85] M. Hjorth-Jensen, *Computational Physics* (University of Oslo, Oslo, 2010).
[86] G. E. P. Box and M. E. Muller, A note on the generation of random normal deviates, Ann. Math. Stat. **29**, 610 (1958).
[87] H. Behringer and R. Eichhorn, Brownian dynamics simulations with hard-body interactions: Spherical particles, J. Chem. Phys. **137**, 164108 (2012).
[88] L. Granger, L. Dinis, J. M. Horowitz, and J. M. Parrondo, Reversible feedback confinement, Europhys. Lett. **115**, 50007 (2016).
[89] L. Dinis and J. M. Parrondo, Extracting work optimally with imprecise measurements, Entropy **23**, 8 (2020).
[90] X. Yang, C. Liu, Y. Li, F. Marchesoni, P. Hänggi, and H. P. Zhang, Hydrodynamic and entropic effects on colloidal diffusion in corrugated channels, Proc. Natl. Acad. Sci. USA **114**, 9564 (2017).
[91] C. Marquet, A. Buguin, L. Talini, and P. Silberzan, Rectified motion of colloids in asymmetrically structured channels, Phys. Rev. Lett. **88**, 168301 (2002).
[92] S. Pagliara, S. L. Dettmer, K. Misiunas, L. Lea, Y. Tan, and U. F. Keyser, Diffusion coefficients and particle transport in synthetic membrane channels, Eur. Phys. J. Spec. Top. **223**, 3145 (2014).
[93] S. Pagliara, S. L. Dettmer, and U. F. Keyser, Channel-Facilitated Diffusion Boosted by Particle Binding at the Channel Entrance, Phys. Rev. Lett. **113**, 048102 (2014).
[94] B. McNamara and K. Wiesenfeld, Theory of stochastic resonance, Phys. Rev. A **39**, 4854 (1989).
[95] L. Gammaitoni, P. Hänggi, P. Jung, and F. Marchesoni, Stochastic resonance, Rev. Mod. Phys. **70**, 223 (1998).
[96] S. Y. Ali, P. Bauri, and D. Mondal, Extraction of work and heat from the bilobal confinement: An entropic stochastic resonance phenomena (unpublished).